Strong collective excitations in low energy neutron scattering from transitional nuclei*

D. F. Coope, S. N. Tripathi, M. C. Schell,† J. L. Weil, and M. T. McEllistrem
Department of Physics and Astronomy, University of Kentucky, Lexington, Kentucky 40506
(Received 21 April 1977)

Elastic and inelastic scattering cross sections for 2.47 MeV neutrons bombarding ^{148,150,152}Sm nuclei were measured. The effects of the stable nuclear deformation on the scattering are unexpectedly pronounced. The inelastic scattering cross sections to the 2^+, 4^+, and 6^+ rotational levels of ^{152}Sm are anomalously large, and there is evidence for excitation of the 8^+ level. The corresponding effect on elastic scattering shows up as large cross-section reductions for ^{152}Sm compared with ^{148}Sm at all angles beyond 60°. The same sort of coupled elastic-inelastic effects are evinced by the ^{150}Sm cross sections, but are less marked. We show that these deformation effects are not explained using the usual coupled-channel optical model. The distribution of inelastic scattering strength to many levels of several shape transitional nuclei shows marked enhancements above statistical model expectations for the collective levels at the expense of cross sections to higher excited levels. The total nonelastic cross sections for all of these nuclei are about equal, indicating that deformation effects principally redistribute the scattering strength to emphasize collective levels strongly coupled to the ground state.

[NUCLEAR REACTIONS ^{148,150,152}Sm(n,n), (n,n'), $(n,n'\gamma)$, E_n=2.47 MeV; measured $\sigma(\theta)$. Coupled-channel model and statistical model analysis.]

I. INTRODUCTION

Low energy neutron scattering from the samarium isotopes, especially the deformed nucleus ^{152}Sm, has proved to be a fascinating study, yielding results which have thus far eluded theoretical description. The elastic neutron scattering angular distributions evince the effects of the varying nuclear deformations of these isotopes. At all angles beyond the forward maximum the elastic scattering cross sections drop dramatically from isotope to isotope, a factor of 2 from ^{148}Sm to ^{152}Sm. These cross-section changes are much too large to be accommodated by a realistic coupled-channel model. However, the greatly *enhanced inelastic* scattering from rotational levels in ^{152}Sm is the most exciting new result of this study. We showed recently[1] that the measured inelastic scattering cross sections cannot be explained using an incoherent combination of direct reaction (DI) and compound system (CS) processes. Our study consisted of measuring scattering cross sections for 2.5 MeV neutrons incident on the nuclei ^{148,150,152}Sm and ^{146}Nd. Most of this paper focuses on the elastic and inelastic scattering measurements made with neutron detection. A separate γ ray detection phase of this study enabled us to investigate level schemes and inelastic scattering cross sections from many excited levels using the $(n,n'\gamma)$ reaction; but only a few results of that work will be reported here.[2]

Only recently have the effects of stable nuclear deformations on neutron scattering been explored. In the past the bulk of attention in fast neutron scattering investigations has been devoted to spherical nuclides, including studies of collective excitations in nuclei that are deformable, but not deformed. Some exceptions are studies done on Si (Ref. 3) and on the actinides.[4] Results discussed in this paper are for ^{148,150,152}Sm, which range from spherical to spheroidal in shape. Figure 1 shows their low-lying levels. The nuclide ^{148}Sm has an almost harmonic excitation spectrum, characteristic of a vibrational nucleus. It is presumed spherical at low excitation energies. On the other hand, ^{152}Sm can be thought of as statically deformed; it has the level structure of a deformed rotor. The excitation character of ^{150}Sm is not clearly either vibrational or rotational. By studying an isotope set comprising such different collective characters we have been able to make comparisons and inferences that would not be possible by studying only one nucleus.

To add perspective to the Sm study presented here, a recounting of recent deformation studies with neutrons is useful. In 1971 Glasgow and Foster[5] published the results of an extensive neutron total cross section survey. A conclusion they drew from this study was that the deformation of the nucleus should be taken into account in the average potential (the optical model potential) used to describe the scattering of neutrons. That this should be done had been suggested as early as 1958 by Chase, Wilets, and Edmonds.[6] Deforming the average potential includes coupling of the elastic channels to exit channels other than just the

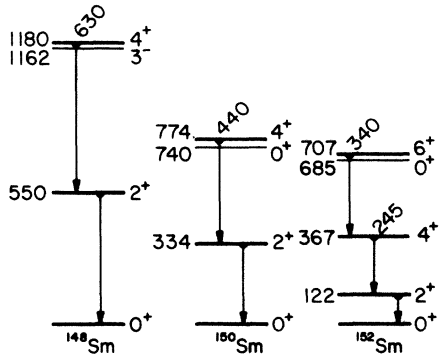

FIG. 1. The low energy portion of the level schemes for ^{148,150,152}Sm. The darker lines represent levels associated with ground state vibrational (^{148}Sm) or rotational (^{152}Sm) excitation modes of the nucleus.

elastic ones. The important channels are identified as collective excitation modes of the nucleus—vibrations and rotations. Neutron total cross section measurements of ^{150,152,154}Sm by Shamu *et al.*,[7] who used separated isotope samples, confirmed that deformation effects could be substantial; that work showed that a coupled-channel representation of the neutron+Sm interaction would produce effects of about the right magnitude. Independently, and at about the same time, Lagrange[8] and Mondin determined potential parameters for some of the rare earth nuclei, including samarium, using a coupled-channel computer program modified from that authored by Tamura.[9] The data base for this determination included s- and p-wave strength functions and some total cross sections for neutrons incident on natural abundance Sm. Later, when this potential was applied to total cross section difference measurements of Shamu *et al.*, it fitted the total cross-section and total cross-section difference measurements beautifully.[10] Only the degree of deformation among the samarium isotopes, the coupling strength, differed markedly from one isotope to the next; the potentials were essentially the same for all Sm isotopes. The depths varied only with the small effects of isospin and neutron bombarding energy dependencies.

Next, studies of fast neutron scattering from ^{148}Sm and ^{154}Sm at 6.25 MeV (Ref. 11) and a more complete study of ^{148,150,152,154}Sm at 7.0 MeV (Ref. 12) were undertaken to determine the deformation effects on *differential* scattering cross sections. The 7 MeV study resolved elastic scattering from the first 2^+ level for all the isotopes except ^{154}Sm. The results showed that as the degree of deformation increases the elastic scattering at large angles decreases by roughly 40% for ^{152}Sm compared with ^{148}Sm. For ^{152}Sm the inelastic scattering angular distributions showed marked structure. Lagrange's coupled-channel potential gives remarkably good agreement[12] with these 7 MeV differential cross sections, both elastic and inelastic. The only deficiency in the model is its failure to produce enough structure in the ^{152}Sm-2^+ angular distribution.

The 7 MeV experiment investigated the scattering at an energy where an extremum in the total cross section difference, $(\sigma_T^{152} - \sigma_T^{148})/\sigma_T^{148}$, had been observed.[10] Another extremum is at about 2.5 MeV, the energy where our interest in the samarium isotopes has centered. At this energy one expects compound system elastic and inelastic scattering to be important in all three isotopes, ^{148,150,152}Sm. If the direct inelastic scattering amplitude is also sizable an extreme interaction model, either direct reaction or compound system formation, should not by itself be expected to represent the results. We shall discuss the problem of combining different reaction mechanisms after discussing the experiment and presenting the measured differential cross sections. Combining calculated intensities incoherently, a procedure usually used successfully,[13] will not work[1] for deformed ^{152}Sm.

This study at 2.5 MeV incident energy was begun with the expectation that the incoherent combination mentioned above would successfully describe the measured cross sections, since the coupled-channel model had worked reasonably well for Sm at 6.25 MeV (Ref. 11) and 7.0 MeV (Ref. 12) where statistical model contributions are negligible. But the present study ends by revealing a strong evolution of the inelastic scattering mechanism from one which in spherical nuclei is insensitive to nuclear dynamics or the nature of the excited levels to one which is dominated by collective effects in soft, deformed nuclei; that is, nuclei whose shapes vary significantly with modest changes in excitation energy.

That the dynamics-insensitive statistical (CS) model is the preponderant description for low energy scattering has been evident for more than 10 years.[4,13-16] Its success has resulted in the use of (n,n') and $(n,n'\gamma)$ reaction studies as powerful tools[14-16] for the assignment of spins to excited levels of nuclei. The effectiveness of this description at low neutron energies has been reasserted[17] in a popular review of recent developments in neutron physics, and this effectiveness is exemplified in a recent study of ^{100}Mo.[16] This nucleus has a large 2^+ deformation-amplitude,[18] $\beta_2 = 0.25$, and a level scheme so compressed from that of the other Mo isotopes that some authors consider it deformed.[16,19] In spite of this, the inelastic scattering cross sections to individual

levels seem to be indistinguishable from those predicted by the CS model.[16]

In the present experiment a markedly different behavior is seen. A rather dramatic and progressive evolution of scattering mechanism occurs away from the traditional behavior[17] to one in which collective properties of nuclear excitations dominate the scattering. This evolution of scattering mechanism will be evident as we examine inelastic scattering to many levels of each of the nuclei ^{146}Nd, ^{148}Sm, and ^{152}Sm. We include some $(n,n'\gamma)$ cross-section measurements[2] so that cross sections are presented for many levels of each nucleus.

II. EXPERIMENTAL PROCEDURE AND DATA UNCERTAINTIES

Both the neutron detection and γ-ray detection phases of this experiment were performed using the University of Kentucky compressed beam-pulse time-of-flight (TOF) facility. The TOF facility is discussed elsewhere[20] and only aspects particular to this experiment will be discussed here. Neutrons were produced using the ^{3}H$(p,n)^3$He reaction. Proton beam bursts from the 6.5 MeV Van de Graaff accelerator were bunched to ~1 ns and directed through a 3.69 mg/cm^2 molybdenum foil into a stainless steel cell containing about $\frac{1}{2}$ atm of tritium gas. A 2 cm diam by about 5 cm high scattering sample was located on the beam axis 12 cm from the end of the gas cell. Neutron flux emanated from the cell with an average energy of 2.47 MeV and an energy spread of 70 keV over the scatterer. The neutron detector, located 3.9 m from the sample, observed scattered neutrons at 13 angles from 20° to 156°. The detector consisted of a 1.3 cm thick by 11.3 cm diam liquid scintillator mounted on a photomultiplier tube. Pulse shape discrimination of neutrons from γ rays was used. The time resolution of the system, as can be seen in the TOF spectrum of Fig. 2, was good enough to resolve well the first excited state of ^{152}Sm at 122 keV excitation energy from the elastic scattering peak. The relative detector efficiency as a function of energy was measured by counting neutrons from the ^{3}H(p,n) source reaction directly at various energies and angles where the reaction cross section is well known. A separate TOF spectrum from a fixed plastic scintillator detector which viewed the tritium neutron source throughout the experiment was used as a monitor. For the γ-ray measurements a 35 cm^3 Ge(Li) detector was used; the experimental procedures concerning the Sm$(n,n'\gamma)$ study are those in regular use in this laboratory[21,22] and will be reported in detail later, when the level and decay scheme studies are presented.[2]

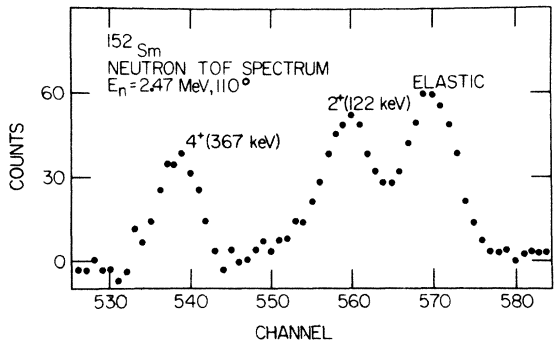

FIG. 2. ^{152}Sm+n time-of-flight spectrum for 2.47 MeV neutrons incident. The spectrum has been smoothed and background contributions have been subtracted. The three peaks are identified with elastic scattering and scattering from the first two excited levels of ^{152}Sm.

The three Sm scatterers used in these measurements were enriched samarium oxide samples (Sm_2O_3) contained in polyethelene cylinders. The samples had had all water driven from them by heating the Sm_2O_3 powder to 800°C for 12–16 h.[12] Table I gives the masses and dimensions. Because elastic scattering from the oxygen and from the polyethelene obstructed samarium elastic and inelastic TOF peaks at some angles, scattering measurements were also made on a water sample and an empty container at each of the angles where samarium oxide scattering was observed. This allowed for the subtraction of the oxygen and carbon scattering contribution after proper normalization. The normalizations of the two types of background runs were corrected for the different attenuations of the different samples. For angles beyond 40° the scattering from hydrogen in the water sample was kinematically shifted out of the region of the TOF spectrum of interest. The spectrum shown in Fig. 2 is one that has been smoothed. That is, each data point of Fig. 2 represents an average over several original channels, the averaging interval being much smaller than the width of any structure present in the data. Also, container and oxide contributions have been subtracted after smoothing them. A peak fitting program which uses a double-Gaussian line shape for each peak[23] was implemented to unfold yields from overlapping

TABLE I. Masses and dimensions of the isotopically enriched samples.

Isotope	Mass (g)	Enrichment (%)	Diameter (cm)	Height (cm)
$^{148}Sm_2O_3$	68.35	96.4	2.0	4.8
$^{150}Sm_2O_3$	47.66	87.4	2.0	3.8
$^{152}Sm_2O_3$	57.63	99.5	2.0	4.7

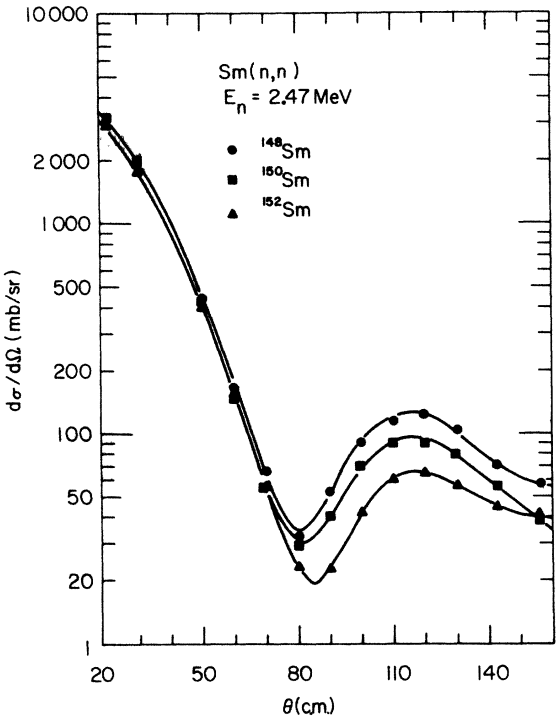

FIG. 3. Elastic scattering differential cross sections for 2.47 MeV incident neutrons on ^{148,150,152}Sm. Cross sections are plotted in center-of-mass coordinates. The curves are Legendre polynomial fits to the measurements.

peaks, as in Fig. 2. The oxygen scattering measurements from the water sample were also used for absolute cross section normalization by comparison with the known ^{16}O total cross section at 2.47 MeV.[24] All cross sections were corrected for dead time losses, geometry, neutron attenuation, and multiple scattering effects.

Uncertainties in our data are of two sorts. The normalization uncertainty is due to the uncertainty in the oxygen total cross section and the uncertainty of the energy dependence of the detector efficiency. These are combined rms to give a normalization uncertainty of 5%. Statistical uncertainty and imperfect background subtraction give uncertainties in the peak yields which vary from angle to angle, called the relative uncertainty. Neither elastic nor inelastic cross sections plotted in figures of this paper show the normalization uncertainty. The relative uncertainties for the measured elastic scattering differential cross sections are typically the size of the symbols used in plotting them in Fig. 3. The relative uncertainties in the inelastic scattering angular distributions are about 7% for ^{150,152}Sm and about 9% for ^{148}Sm. The latter is most affected by background subtraction uncertainties because the elastic scattering peaks from carbon and oxygen occur in the same part of the TOF spectrum as the peak for inelastic scattering to the 2^+ level of ^{148}Sm at angles beyond 80°. For angles smaller than 40° the hydrogen elastic scattering made extraction of the ^{148}Sm-2^+ yield impossible; this was also true for ^{150}Sm at 20°. At 20° and 30° inelastic scattering from the ^{152}Sm-2^+ level could not be separated with any precision from the enormous elastic peak. Errors in our multiple scattering and attenuation corrections are believed to introduce uncertainties of about 1% each in the corrected cross sections. These corrections take into account the wide ($\Gamma = 124$ keV) ^{16}O+n compound nucleus resonance,[24] which is manifest in the O total cross section as a large dip at 2.35 MeV. The attenuation and multiple scattering corrections are made with two methods. One uses an approximate, analytic procedure developed by Engelbrecht[25] and the other uses a Monte Carlo method originally developed at ORNL[26] and extended by Velkley *et al.*[27] The two methods gave corrected cross sections which agreed with one another to within 1%, or corrections which agreed to within 4%.

III. MEASURED CROSS SECTIONS AND WOLFENSTEIN-HAUSER-FESHBACH CALCULATIONS

Elastic scattering differential cross sections for 2.47 MeV neutrons bombarding ^{148,150,152}Sm are presented in Fig. 3. The solid curves are Legendre polynomial fits to these data; the attendant Legendre polynomial coefficients to these fits and the fits to the inelastic scattering data are given in Table II. The systematic effects of the varying nuclear deformation on the scattering are indicated by the pronounced differences of the back-angle cross sections. These differences are much more dramatic than was observed at higher energies.[12] Moreover, they cannot be explained as compound elastic scattering or isospin dependent differences in the potential, as we shall show.

TABLE II. Legendre polynomial coefficients for the fits of the ^{148,150,152}Sm+n elastic and inelastic (2^+) measured differential scattering cross sections. Units are mb.

	^{148}Sm		^{150}Sm		^{152}Sm	
Order	Elastic	2^+	Elastic	2^+	Elastic	2^+
0	400	40.1	386	39.0	353	47.8
1	832	···	845	10.1	796	22.1
2	1051	···	1066	3.80	997	7.55
3	985	···	977	···	894	3.40
4	610	···	638	···	577	−24.6
5	312	···	340	···	311	−19.9
6	170	···	167	···	154	···
7	58.2	···	48.7	···	48.9	···

Spherical optical model representations of the measured elastic scattering cross sections were attempted first, using the computer code ABACUS II (revised).[28] We refer to these as "one-channel" calculations since no explicit coupling between channels is included. The purpose of these one-channel calculations was twofold. First, to show that the average potentials necessary to represent the data demonstrate that in the deformed region the effect of channel coupling is a major influence on the potential (which includes the coupling implicitly), especially at 2.5 MeV incident energy. The influence of strong coupling on one-channel potentials for higher incident energies has been explored in some detail in an earlier publication, dealing with 6–10 MeV neutron scattering from the highly deformable Se isotopes.[29] Secondly, the requisite scattering amplitudes, η_l, generated to fit the elastic scattering cross sections were used in a Wolfenstein-Hauser-Feshbach[30] (WHF) calculation to predict contributions to the scattering from compound system (CS) processes, both elastic and inelastic cross sections, for all three Sm isotopes. Although for the ^{152}Sm+n interaction channel coupling is strong, as we shall show, it is not incorrect or inaccurate to derive the amplitudes η_l from a one-channel model which fits the elastic scattering cross sections. The values of η_l are highly constrained by requiring that a model provide a good fit to the elastic scattering cross sections, independent of the particular optical model used—one-channel or coupled-channel. That this is, in fact, true is shown explicitly in the Appendix to this paper.

The calculated compound elastic cross sections used have included the level width fluctuation correction of Satchler[31] and Moldauer.[32] The value 1.7 for the correction factor is determined in this laboratory to be most satisfactory in describing low energy neutron scattering cross sections in the mass region $A \sim 90$ and other mass regions.[20] The compound elastic contribution is small, about 11 mb/sr for ^{148}Sm and 3 mb/sr for ^{152}Sm, so that uncertainty in this correction factor is relatively unimportant. The calculated inelastic cross sections, on the other hand, were not corrected for either the possible enhancement of the inelastic scattering due to channel correlation effects or the loss of inelastic scattering due to the enhancing of the CS elastic scattering. Moldauer has explained[32] that these effects approximately cancel in the inelastic channels.

The derived one-channel fits to elastic scattering, including the CS contributions, are shown in Fig. 4 for ^{148,152}Sm; for visual clarity the ^{150}Sm fit is not shown, but its agreement with the measurements is comparable to those for ^{148,152}Sm.

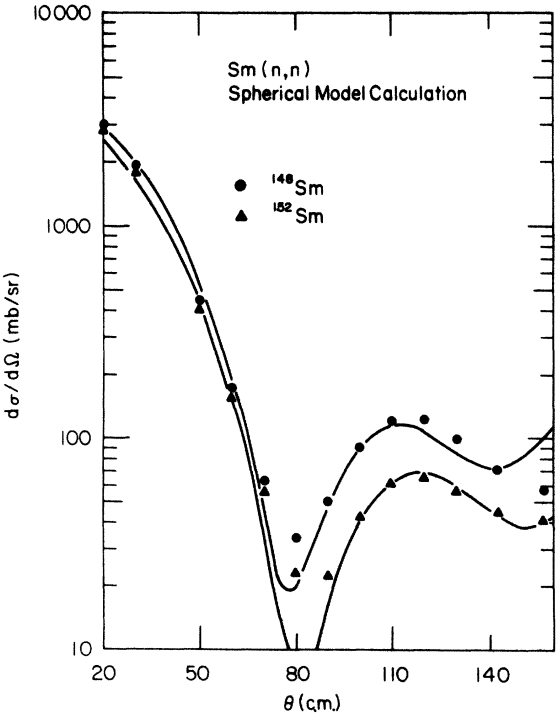

FIG. 4. Spherical-optical (one channel) model representations of the ^{148,152}Sm elastic scattering cross sections. The potential depths and form factors used to calculate these cross sections are given in Table III; the calculations are discussed in the text. The symbols represent the measurements.

The potential depths and form factors for all three isotopes are given in Table III. These potentials are ones which best reproduce the elastic scattering; they overestimate the total cross sections by about 6%. The parameters are not unique, and we were able to obtain other equally good fits using different potentials and geometries. However, as stated above these potentials should all be expected to predict the same CS scattering cross sections, and explicit tests show that they do. The particular fits given in Fig. 4 and in Table III were chosen because they use the same form factors as the coupled-channel calculations to be discussed later.

It was suggested by Glendenning, Hendrie, and Jarvis[33] that scattering from an isotope set should be described by a potential that differs from one isotope to the next only in its isospin dependence and its accountability for the nuclear deformation. However, the depths of the real part of the scattering potential we have derived from the spherical model would imply an isospin dependence of 1 MeV, twice as large as any previously suggested value, and thus unreasonable. Furthermore, the 2.7 MeV disparity in the imaginary potential depths is even further from expected behavior. Thus,

TABLE III. Optical model parameters used in calculations discussed in the text. The potential form is given by Eq. (1). The geometrical parameters were $R_0 = 1.25A^{1/3}$, $a = 0.65$, and $a' = 0.58$ for all calculations except the lighter curves in Fig. 9; they had $R_0 = 1.23A^{1/3}$. A is the atomic mass number and all dimensions are in fm. All the calculations used a spin-orbit potential depth of 8.5 MeV.

Model		Nucleus	Potential depth (MeV) Real	Imaginary	Deformation parameters
One-channel model	Fig. 4	^{148}Sm	47.0	3.8	
	not shown	^{150}Sm	46.5	5.0	
	Fig. 4	^{152}Sm	46.0	6.5	
0^+-2^+ CC model of Ref. 12	Fig. 8	^{148}Sm	46.6	3.74	$\beta_2 = 0.14$
	not shown	^{150}Sm	46.4	3.64	$\beta_2 = 0.17$
	Fig. 8	^{152}Sm	46.2	3.54	$\beta_2 = 0.22$
0^+-2^+-4^+-6^+ CC model	Fig. 9 (darker curve)	^{152}Sm	46.2	2.5	$\beta_2 = 0.22, \beta_4 = 0.02$
	Fig. 9 (lighter curve)	^{152}Sm	46.8	2.0	$\beta_2 = 0.27, \beta_4 = 0.02$
0^+-2^+-4^+ CC model	Fig. 9 (dashed curve)	^{152}Sm	46.2	2.5	$\beta_2 = 0.23, \beta_4 = 0.02$

these one-channel calculations seem to reveal the effects of the nuclear deformation indirectly, in that the measured elastic scattering cross sections require one-channel potentials which are inconsistent with known systematic dependencies.

As noted earlier,[1] the effects of nuclear deformation are most striking in the ^{152}Sm inelastic scattering measurements; they are evinced by the familiar direct interaction (DI) structure of the angular distributions and by the strong enhancements over WHF expectations of the inelastic scattering cross sections. That the cross sections are unusually large is clear upon inspection of Figs. 2 and 5. The neutron TOF spectrum (Fig. 2) shows scattering peaks for the 2^+ and 4^+ levels that are comparable in size with the elastic peak; and this is at an angle where the elastic scattering is at a relative maximum. Figure 5 is a γ-ray

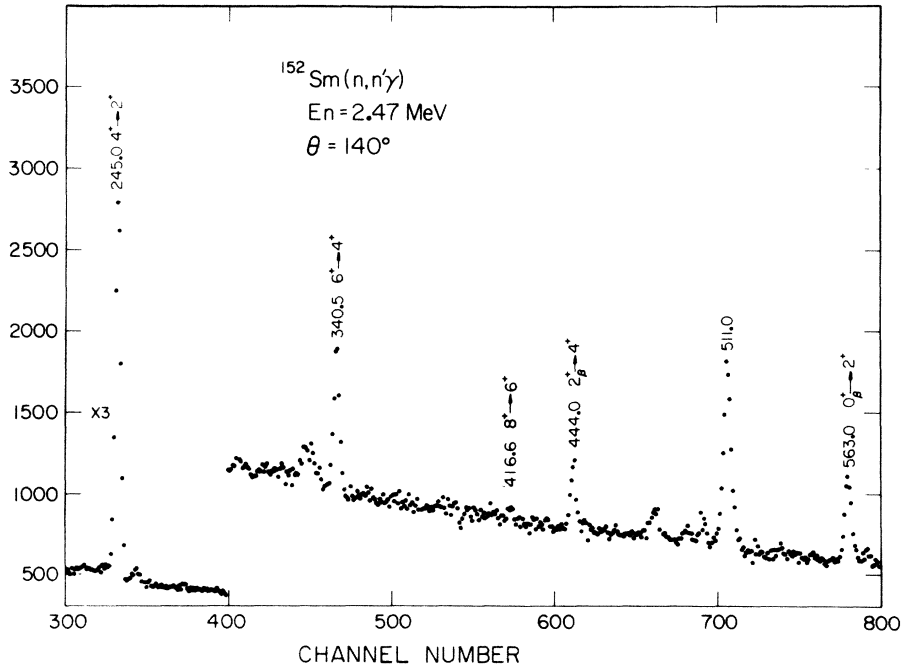

FIG. 5. $(n,n'\gamma)$ photon spectrum for 2.47 MeV neutrons incident on $^{152}Sm_2O_3$. Peaks in the spectrum are identified with electromagnetic transitions between levels of ^{152}Sm, as specified in the figure. Although the 416.6 keV peak is not readily evident in this spectrum, it is consistently present in the spectra for all angles where scattering was observed.

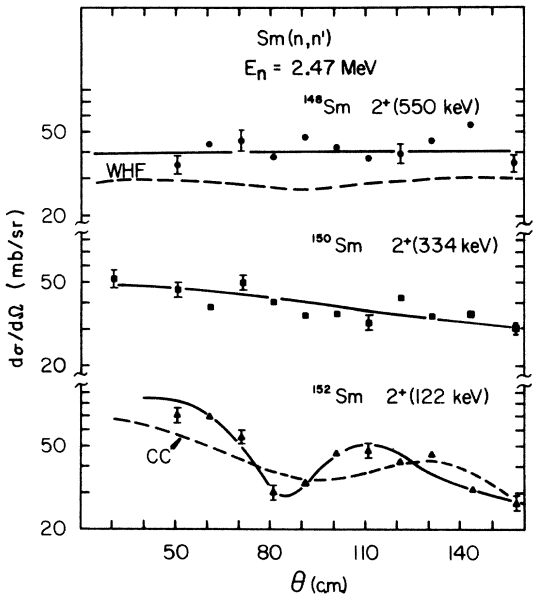

FIG. 6. Inelastic scattering cross sections from the first 2^+ levels of ^{148,150,152}Sm for an incident neutron energy of 2.47 MeV. The cross sections are plotted in center-of-mass coordinates. Solid lines are Legendre polynomial fits to the measurements; dashed curves represent theoretical calculations described in the text.

spectrum from our ancillary ^{152}Sm$(n,n'\gamma)$ study. One sees there prominent peaks associated with the excitation of the 4^+ and 6^+ levels with 2.47 MeV incident neutrons. A γ ray associated with the $8^+ \rightarrow 6^+$ (416.6 keV) transition is also observed. However, another transition is known of about the same energy in ^{152}Sm.[34] We have corrected the intensity of the 416.6 keV γ ray to obtain

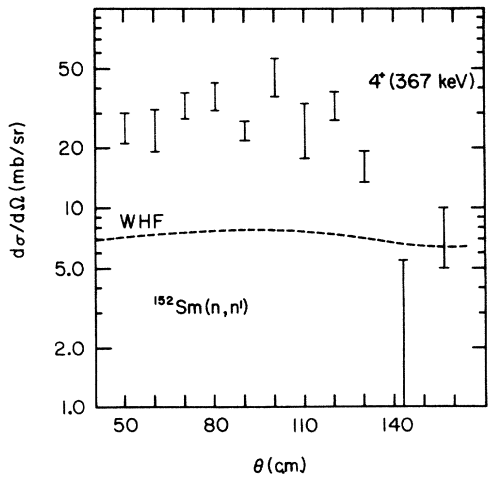

FIG. 7. Inelastic scattering cross section from the 4^+ (367 keV) level of ^{152}Sm for an incident neutron energy of 2.47 MeV. The dashed curve represents a theoretical calculation described in the text.

the cascade feeding to the 6^+ level.

Differential scattering cross sections for inelastically scattered neutrons from the 2^+ and 4^+ levels of ^{152}Sm are shown in Figs. 6 and 7. Figure 6 also shows the ^{148,150}Sm-2^+ cross sections. The solid curves are Legendre polynomial fits to these angular distributions. Evident is the marked structure of the ^{152}Sm-2^+ cross section, with the cross section ranging over a factor of 3 from forward peak to minimum; this structure fades for ^{150}Sm, and is absent for ^{148}Sm. The fore-aft asymmetry of the angular distribution is the signature of direct scattering. Compound inelastic scattering would be symmetric about 90°, with little anisotropy. The WHF contribution to the ^{148}Sm-2^+ cross section is represented by the dashed curve in Fig. 6; it comprises about 70% of the measured cross section. For ^{150,152}Sm the WHF cross sections are not shown because they are small, less than 15 mb/sr each. The angular distribution for inelastic scattering from the ^{152}Sm-4^+ level, Fig. 7, also demonstrates a DI pattern, the cross section falling off abruptly in magnitude at angles beyond 120°. The WHF calculation for this level is shown as the dashed curve.

Enhancements of the measured angle-integrated cross sections above WHF expectations for inelastic scattering from ^{152}Sm are indicated in Table IV. There the neutron detection and $(n,n'\gamma)$ cross sections are compared with each other and contrasted with results of our WHF calculations. The agreement between the cross sections measured with two different detection methods for the 4^+ level of ^{152}Sm is very good, and contributes to the confidence with which the measurements are viewed. As mentioned above, the neutron detection results are normalized to the known O scattering cross sections,[24] whereas the $(n,n'\gamma)$ results are normalized to a compilation[22] of γ-ray production cross sections for the 846.7 keV line in ^{56}Fe; the agreement shown in Table IV is one of independently determined results. The measured cross sections are a factor of 3–4 larger than WHF estimates for the levels of ^{152}Sm listed in Table IV. This study presents clear and unambiguous evidence of the dominance of direct inelastic scattering at low neutron energies. Since our first reports[1,35] of this dominance, similar observations have been reported in the actinide region[16,36] by others.

IV. COUPLED-CHANNEL CALCULATIONS

The preceding section showed directly the effects of nuclear deformation on elastic and inelastic neutron scattering. The elastic scattering an-

TABLE IV. Measured inelastic scattering cross sections for ^{148,150,152}Sm compared with CC and WHF calculations. The CC cross sections are calculated for ^{148,150}Sm using the potential given in Ref. 12, and for ^{152}Sm using the potential represented in Fig. 9 by the darker curves. All cross sections are in mb.

		Measured		Theory		
Isotope	Level	(n,n')	$(n,n'\gamma)$	WHF	CC	WHF+CC
^{148}Sm	2^+	504±40	···	352	277	629
^{150}Sm	2^+	491±30	···	227	439	666
^{152}Sm	2^+	600±40	···	140	533	673
	4^+	271±30	263±35	94	65	159
	6^+	···	61±10	23	9	32
	8^+	···	7± 2	0.6	···	···

gular distributions vary systematically among the Sm isotopes with varying nuclear deformation. For the deformed rotor ^{152}Sm scattering from the ground state rotational band is enhanced, certainly via coupling with the incoming channel. We expected that these results should be understandable within the context of a coupled-channel (CC) model. Such is not the case. As already discussed, potential parameters for a two-level model (0^+-2^+) have been determined for the Sm isotopes by Lagrange to fit total cross sections from 0.4 to 14 MeV and strength functions.[10] Predictions of this model agree well with the scattering measurements at 7 MeV,[12] and so we applied it to our results. The potential has the form

$$V(r,\theta) = -Vf(r,a,R) + iW_D 4a' \frac{d}{dr} f(r,a',R) + V_s \vec{\sigma}\cdot\vec{l}\,\frac{d}{dr} f(r,a,R_0)\,. \quad (1)$$

The form factor is given by the expression $f(r,a,R) = [1+\exp(r-R)/a]^{-1}$ with $R = R_0(1+\sum_\lambda \beta_\lambda Y_{\lambda 0}(\theta))$ generally, and $R = R_0(1+\beta_2 Y_{20})$ for the 0^+-2^+ model discussed there.[10,12] The parameters of these potentials are given in Ref. 12, and their particular values at 2.5 MeV are given in Table III. We stress here that the potential differs among ^{148}Sm, ^{150}Sm, and ^{152}Sm only in its isospin dependence. The attendant coupling strengths to this analysis are $\beta_2 = 0.14$, 0.17, and 0.22 for ^{148,150,152}Sm, respectively. CC calculations using this model at 2.47 MeV for ^{148}Sm and ^{152}Sm are shown in Fig. 8. The points are our elastic data with the corrected CS elastic contribution subtracted for both isotopes. The CC representation for ^{150}Sm is not shown; it lies between the two curves in Fig. 8, regardless of the choice of coupling scheme chosen—vibrational or rotational.

The ^{152}Sm angular distribution is well represented by the 0^+-2^+ CC model (solid curve) but the ^{148}Sm (dashed curve) and ^{150}Sm predictions fail. This model predicts that there is little difference in the elastic scattering among the three isotopes; in fact, the model predicts that channel coupling has a small effect on the elastic scattering at 2.5 MeV.

As seen in Table IV, the 2^+ inelastic cross sections for all three isotopes are also fairly well fitted, to within about 25%, by the two-level Lagrange model and WHF cross sections added. The

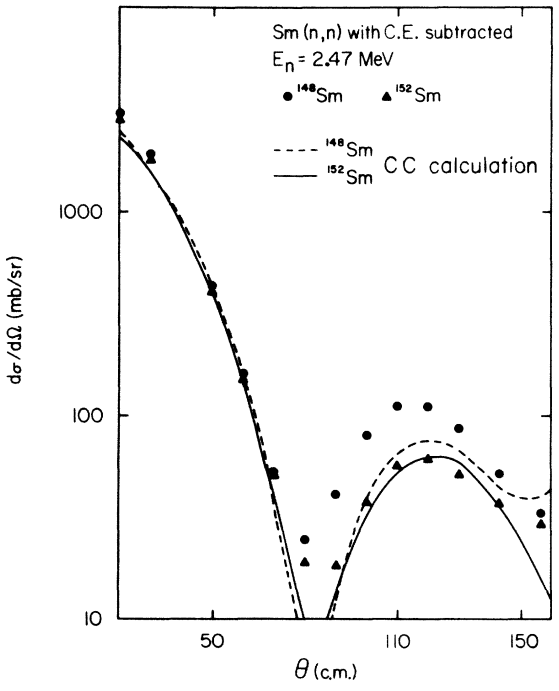

FIG. 8. Coupled-channel model representations of the ^{148,152}Sm elastic scattering cross sections. The potential depths and form factors used to calculate these cross sections are given in Table III; the calculations are discussed in the text. The symbols represent the measured elastic cross sections with an enhanced *compound elastic contribution subtracted* at each angle.

CC calculation is shown in Fig. 6 for ^{152}Sm; the WHF cross section is not added to the CC prediction in that figure. A significant deficiency of the 0^+-2^+ coupled-channel model is its failure to provide enough structure in the 2^+ angular distribution. The same problem arose with the 7 MeV ^{152}Sm(n,n') angular distribution.[12] This pronounced structure could be the effect of the coupling of other higher spin channels to the 2^+ channel. We stated in the previous section that the 4^+ and 6^+ cross sections are unexpectedly large, and thus it is not surprising that a model that does not explicitly consider that these other channels would have some weaknesses.

Our attempts to predict the elastic and inelastic neutron scattering cross sections for ^{152}Sm include coupling the 0^+, 2^+, 4^+, and 6^+ channels through both quadrupole and hexadecapole deformation. We shall demonstrate our conclusion, that no choice of potential or deformation parameters provides a good representation of the data. Because the CC calculations do not reproduce the data well, we will outline the general directions taken in our exhaustive search for a satisfactory fit. The constraints that define an acceptable fit are as follows: (1) The total cross section at 2.47 MeV, 6.3 ± 0.2 b,[10] should be well reproduced since it is linear in the scattering amplitudes; failure to fit it implies incorrect amplitudes. (2) The elastic, 2^+, and 4^+ angular distributions should be reproduced. The 6^+ inelastic cross section need only be fitted in magnitude; we have not measured the neutron angular distribution for scattering to the 6^+ level. The 8^+ was not included in our calculations.

One might suppose that the coupling strength parameters β_λ correspond directly to the nuclear deformation and can therefore be taken from electron scattering or Coulomb excitation measurements. In our calculations, however, the β's were treated rather as initial values in a search, since the issue in this analysis was obtaining any reasonable description of the measured cross sections, and not specifying β parameters.

The first calculation to be discussed is an extension of Lagrange's 0^+-2^+ model by including the 4^+ and 6^+ channels and β_4 coupling. Including the effects of these channels explicitly should necessitate reduction of the imaginary potential depth from the two-level model. It was reduced from 3.5 to 2.5 MeV. The heavy solid curves of Fig. 9 are the calculations thus obtained. One notes that the fits to the elastic data are inferior to those of the 0^+-2^+ model. All of the experimental points shown have calculated WHF contributions subtracted from them to facilitate comparison of the CC calculations with measurements. The coupling

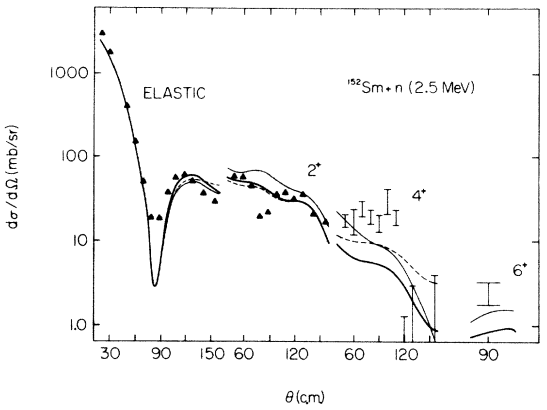

FIG. 9. Coupled-channel calculations for ^{152}Sm discussed in the text. The measured differential cross sections, represented by the solid triangles and by the error bars, have CS contributions subtracted. The 6^+ cross section is represented by the measured value (minus a CS contribution) divided by 4π. The solid lines represent four-level calculations, the dashed curves represent a three-level calculation.

strength β_4 used here is not the one expected from charged particle or electron scattering measurements, but instead one that gives a better fit, $\beta_4 = 0.02$. This four-level model fails to predict the 4^+ and 6^+ cross sections both by roughly a factor of 3 and represents the elastic and 2^+ angular distributions poorly. Were β_4 to be increased, the 2^+ cross sections would become much too large. Of course, the Lagrange potential parameters were developed within the framework of a two-level model, so the failure of that potential to represent our cross sections may not be surprising. However, if only the form factors (or geometrical parameters) are retained and all other parameters are permitted to vary over wide ranges, the *best* fit that can be derived is no better and not much different from the calculation just discussed. The difficulty in fitting measurements for all of the levels seems to be endemic to the model used. Simply stated, the problem is that in order to increase the predicted 4^+ and 6^+ cross sections one must increase the coupling strengths, β_2 and β_4, and/or decrease W_D, the imaginary potential. However increasing the coupling strength generally increases the total cross section. Furthermore, the predicted structure of the elastic and inelastic angular distributions, and especially the 2^+ angular distribution, is sensitive to β_2 and β_4. Increasing the β's or decreasing W_D will make the fit to the angular distributions even worse than those of Fig. 9. The imaginary potential produces the calculated inelastic scattering that is not explicitly produced by the coupling. The effect of reducing W_D is to increase cross sections of explicitly coupled channels, which is desirable, but this also increases

the total cross section to unacceptably high values.

In another test of the CC model we altered the form factors. The effect of the imaginary potential on the scattering can be reduced by decreasing the imaginary radius in the form factor. This allows the coupling strength to be increased, while keeping the calculated total cross section close to the experimental value. Our best fit using a different geometry is represented by the lighter solid curves of Fig. 9. This calculation uses a much larger β_2 than the Lagrange one, even when one corrects[37] for the different form factor. The fits to the 4^+ and 6^+ cross sections are improved, but the elastic and 2^+ fits are unacceptable.

Other approaches, such as including β_6 or adding more channels, were tried to no avail. For instance, the dashed set of curves in Fig. 9 show the effect of deleting the 6^+ level to produce a 0^+-2^+-4^+ calculation. The 4^+ cross section is increased by a factor of about 2. The point is, increasing the model space worsens the fits. It is important to realize that, although the 0^+-2^+-4^+ calculation comes closer to fitting the 4^+ measured cross section than does the four-level model, it is still well below it. This is not so evident in Fig. 9 because of the compactness of the logarithmic cross-section scale.

We must conclude that neutron scattering at 2.5 MeV from the deformed nuclide ^{152}Sm cannot be understood as the incoherent admixture of CC and WHF cross sections. At energies where both direct and compound system processes compete, and in nuclei where the nuclear deformation apparently enhances correlations among channels, the assumption that outgoing "flux" should be statistically distributed is a poor one. Introducing these correlations explicitly in a calculation, or using the methods of Engelbrecht and Weidenmüller *et al.*[38] and of Moldauer,[32] which allow direct and CS processes to interfere, might explain the observed inelastic scattering. However, the interference effects will have to be quite large, which is unexpected[32] since many channels are open and strongly coupled,[2] as described below. In the many-channel limit, all such corrections become quite small.

A recent neutron scattering experiment[36] on ^{232}Th, also at 2.5 MeV incident energy, measured 2^+ and 4^+ inelastic scattering cross sections and represented them with CC model calculations. Because of the large number of levels in ^{232}Th below 2.5 MeV, the CS contributions to the 2^+ and 4^+ levels are negligible. The apparent success[16,36] of the CC model in the actinide region may lend support to the hypothesis that the problem in the Sm isotopes results from interference between reaction amplitudes.

In a companion ^{152}Sm$(n,n'\gamma)$ study we have observed[2] enhanced scattering to levels of the β, γ, and octupole vibrational bands, as well as the results shown for the ground state band in Table IV. Andreev, Basenko, and Sit'ko[39] have reported similar findings. We have also made measurements for scattering to excited levels in ^{146}Nd and ^{148}Sm.[2] After correcting the γ-ray production cross sections for cascades from higher levels, and for sample-size effects,[40] we obtain neutron inelastic scattering cross sections for more than 15 levels in each nucleus. The deviations of these measured cross sections from WHF model expectations are shown in Fig. 10, in which the ratio of measured to WHF cross section is plotted as a function of excitation energy for each nucleus. Included at the bottom of the figure are deviations for ^{94}Zr, taken from an extensive study[21] of neutron inelastic scattering in ^{92}Zr and ^{94}Zr, both rigidly spherical. In that study some 27 cross section measurements near 3 MeV incident energy showed an average deviation of model from measurement of about 25%. The results for ^{94}Zr alone in Fig. 10 are better than this, consistent with the reassertion of the dominance of the statistical model by Sheldon and Feshbach,[17] and by others.[16] One sees for ^{146}Nd and ^{148}Sm a systematic departure, with developing enhancements for the low-lying collective levels at the expense of cross sections to higher levels. The enhancements and depletions are evident in ^{146}Nd, but considerably more marked in ^{148}Sm. The neutron separation energies of the Nd isotopes are somewhat larger[41] than those for their isotones in Sm. This and other evidence suggests that the Nd isotopes tend toward deformation at a slower rate than their Sm isotones. Thus ^{146}Nd should be less deformable than ^{148}Sm, consistent with the different enhancements and depletions of Fig. 10. Finally in ^{152}Sm the enhancements reach a factor of 4 for members of the ground state band. A very interesting property of these results for Nd and Sm isotopes is that the nonelastic cross section, or sum of inelastic scattering cross sections, is ~1.2 b for all of the isotopes, ^{146}Nd and ^{148,150,152}Sm. The message of the enhancements and depletions of Fig. 10 is that the deformation effects simply account for a redistribution of the absorbed flux, increasingly far from WHF expectations as the deformability of the nucleus increases.

V. CONCLUDING REMARKS

The effects of stable nuclear deformations on low energy neutron scattering are unexpectedly pronounced. The inelastic scattering cross sections to rotational levels of ^{152}Sm are anomalously

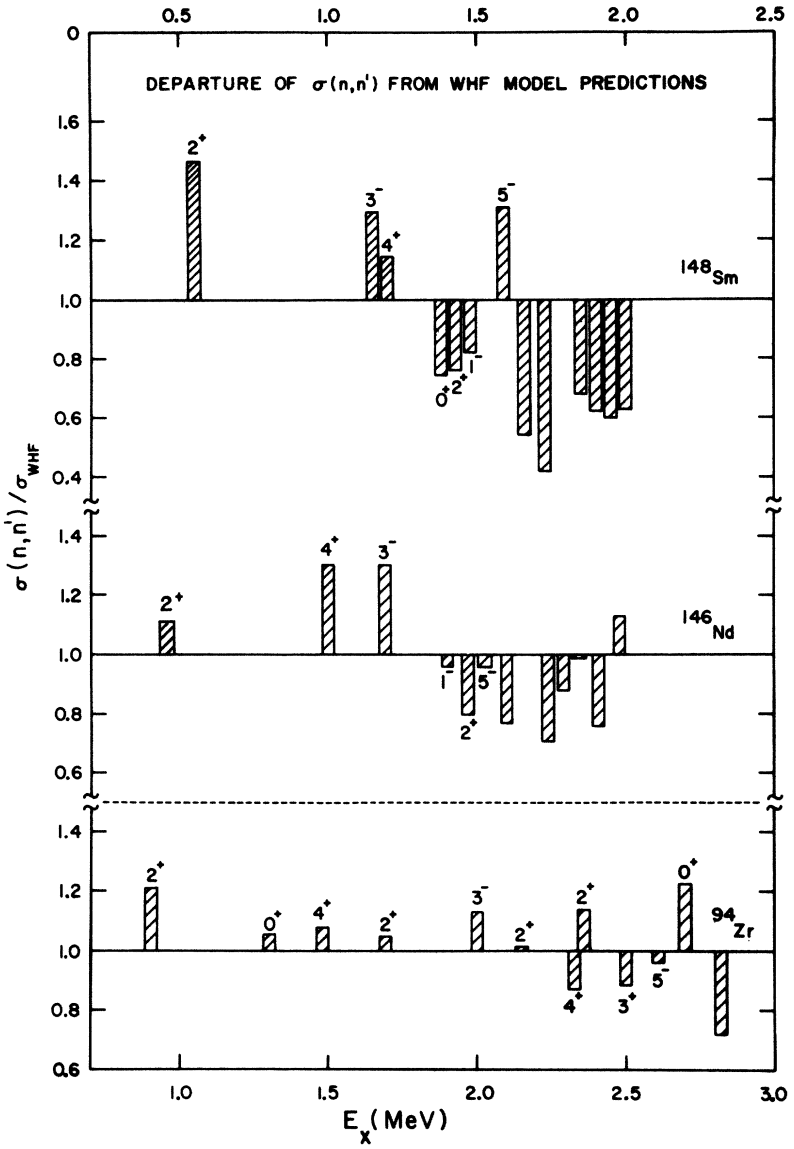

FIG. 10. Ratios of measured to WHF model inelastic scattering cross sections plotted as a function of energy for levels of ^{146}Nd, ^{148}Sm, and ^{94}Zr. Deviation from 1.0 represents the amount of enhancement or depletion of the inelastic scattering compared to that expected from the WHF statistical model.

large, with correspondingly large effect on the elastic scattering differential cross sections. The effect on elastic scattering shows up as cross-section reductions at all angles beyond 60°. The same sort of coupled elastic-inelastic effects are also evident in ^{150}Sm, but are much less marked in that nucleus.

The deformation induced coupling is characterized by the coupling parameters β_2 and β_4, which ultimately we would like to consider as characteristics of the target nucleus, or at least of the neutron-nucleus interaction. In the present study it is clear that such attribution would be unreasonably presumptuous, although precisely that sort of characterization did seem reasonable in earlier studies of total neutron cross sections for these isotopes,[10] and also in a study of elastic and inelastic scattering[12] at much higher incident energy. If, as we suspect, the failure of the analysis in this work reflects correlations between statistical model amplitudes induced by the presence of directly coupled amplitudes, the problem may be particular to the 2–4 MeV incident energy region, where both amplitudes are comparably large. Total cross sections, which do not separate elastic and inelastic scattering cross sections, may not be

sensitive to such correlations. The differential scattering cross sections at 7 MeV incident energy[12] contain no appreciable compound system component.

Finally, we would like to underscore the importance of the comparative technique of scattering from both spherical and deformed isotopes, to see directly the effects of stable deformations on both elastic and inelastic scattering. In fact, this comparative technique was used earlier by Shamu *et al.* in their exposition of deformation effects in total cross sections.[7,10] It was important also to use both neutron and γ-ray detection methods so that the strong enhancements of neutron inelastic scattering cross sections to many levels could be separately observed. The relatively complete data set enables us to see and measure coupling phenomena that a more fragmentary study would not have revealed. Future analysis efforts will be directed towards testing models which specify correlations induced by direct reaction amplitudes.

The authors gratefully acknowledge the loan of the separated Sm_2O_3 samples from the Research Materials Collection of the Isotope Sales Center, Oak Ridge National Laboratory.

APPENDIX

We discuss here three special aspects of our WHF[30] calculations that are not of a routine nature. These three considerations are designed to make certain that the calculations are fully valid within the context of a coupled-channel model, as opposed to the usual one-channel calculations, and also to provide a correction for unobserved excited levels; these considerations lead to small corrections which are often ignored when a test of the applicability of the WHF model is not one of the central issues. Sections A and B detail: (1) the method used to estimate level densities for ^{148,150,152}Sm so as to ascertain the number of unobserved levels, and (2) the procedure used to accomodate the large number of levels (about 65 for both ^{150}Sm and ^{152}Sm) in the calculations. Section C discusses the method used by us to determine the transmission coefficients needed for all channels. A detailed discussion of our methods is given because these calculated WHF cross sections were subtracted from measured differential cross sections before attempts were made to represent the scattering with the coupled-channel model. We expect that the calculated cross sections are correct to within about 10%, although a large error, 25% or so, in these calculations would not really affect the conclusions of this article. For instance, the WHF cross section for scattering to the ^{152}Sm-4$^+$ level is about 8 mb/sr, whereas the measured cross section is around 22 mb/sr. A 25% uncertainty in the WHF calculation would increase the overall uncertainty in the 4$^+$ direct interaction cross section about 15%; but the CC model representation of the data, Fig. 9, is deficient by a factor of 2.

A. Estimating the number of levels

The distributions of levels for the isotopes ^{148,150,152}Sm were estimated using the Gilbert-Cameron level density formula[42] suitable for excitation energies below 5 MeV. For these low energies it has the simple form,

$$\rho(E,J) = [(2J+1)/2\sigma^2]\exp[-(J+\tfrac{1}{2})^2/2\sigma^2]\rho(E)\,, \qquad \text{(A1)}$$

where

$$\rho(E) = T^{-1}\exp[(E-E_0)/T]\,. \qquad \text{(A2)}$$

The excitation energy and spin of the level are E and J; σ^2, the spin cutoff parameter, T, the nuclear temperature, and E_0 are empirical numbers taken from Ref. 42 and are given in Table V for each isotope. This simple level density expression assumes that the distribution of spins is energy independent and that even or odd parity levels are equally likely. Table V also gives the fraction of each spin present through spin $J=6$ for the three isotopes. Higher spin levels need not be considered because calculated cross sections to them would be insignificant, as one can see in Table IV.

Integrating the formula, Eq. (A1), over various energy intervals gives a prediction for the number of levels of all spins in those energy intervals. We compare in Table VI the predictions of Eq. (A1) with numbers of levels presently known below the given energies. Only levels through spin 6 are included. Inspection of the table shows that agreement is fairly good between Eq. (A1) and the data below 2.5 MeV for ^{148}Sm, below 1.5 MeV for ^{150}Sm, and below 2 MeV for ^{152}Sm. Above 2 MeV the calculation predicts more levels than have been observed for both ^{150}Sm and ^{152}Sm, as would be expected since as the excitation energy increases experimental sensitivity generally decreases. We therefore accept the predictions of Eq. (A1) as a good estimate of the level density below 2.5 MeV and use the results of Tables V and VI in Sec. B of this appendix.

B. Correcting the WHF calculations for many levels

The previous section showed that there are a large number of levels in ^{150}Sm and ^{152}Sm below 2.5 MeV. The first 10 or 15 levels of ^{150}Sm and ^{152}Sm, and almost all of the levels in ^{148}Sm, are well established, and the statistical model predicts that the cross sections for decay of the compound

TABLE V. Level density parameters from Ref. 42 and spin dependent factor of Eq. (A1) evaluated for spins $J=0$ through $J=6$.

	T	E_0	σ^2
^{148}Sm	0.54	0.7	21
^{150}Sm	0.555	−0.08	26
^{152}Sm	0.55	−0.08	27

Spin (J)	^{148}Sm	^{150,152}Sm
0	0.023	0.018
1	0.067	0.054
2	0.102	0.084
3	0.124	0.108
4	0.132	0.116
5	0.127	0.117
6	0.113	0.110
Sum 0–6	0.69	0.61

system to these low-lying levels is fairly insensitive to the character of any one level above. Therefore using the level number predictions in Tables V and VI should enable us to make very good estimates of the WHF cross sections to the low-lying levels of interest.

Because the computer code[28] that we used to calculate WHF cross sections can handle only 25 levels, a special method was necessary to correct the results for the many other levels. This was done rather than increasing the level capacity of the program because it is much simpler and just as accurate. The correction procedure was basically to include all the levels, e.g., 66 for ^{152}Sm, but to include them in a number of calculations done separately. In each calculation the same 15 lowest energy levels were always included, together with 10 additional levels. These 10 levels were grouped in energy intervals of width $10/\rho(E)$. Spin values were distributed according to Table V; even and odd parities were equally assigned. The calculation was repeated enough times to cover all of the presupposed levels, each time centering the energy interval containing the new levels at an increasing excitation energy, up to 2.5 MeV. In this way, the effects of these higher energy levels on the lower ones were inferred. These separate, 25-level calculations gave the distribution of inelastic scattering cross sections as a function of excitation energy. When this distribution was normalized to the nonelastic cross section, the inelastic scattering cross sections to the low-lying levels of interest were correctly determined.

TABLE VI. Comparison of the number of levels for ^{148,150,152}Sm determined both using Eq. (A1) and counting known levels. Only levels up to spin 7 are included.

	^{148}Sm		^{150}Sm		^{152}Sm	
E (MeV)	Known	Calc.	Known	Calc.	Known	Calc.
<1.0	1	1.0	3	3.6	8	3.6
<1.5	4	2.8	7	9.8	17	10
<2.0	9	7.5	11	25	26	26
<2.5	19	19	15	63	···	66

This procedure is correct to within a few percent, if compared with a WHF evaluation that actually included 65 levels simultaneously. Our confidence in this statement is partly based upon test calculations for a nucleus with 24 levels. Three test calculations were done including 15 low-lying contiguous levels and 3 of the 9 remaining levels, so that the 3 calculations included all 24 levels. This was compared with a single calculation including all 24 levels simultaneously. The σ_{2^+} calculated in these two ways agreed with one another to better than 1%.

C. Transmission coefficients

The cross section for scattering through the compound system to a particular channel is entirely determined by the transmission coefficients and the energies and spin-parities of the open channels. That is the essence of the statistical model. The transmission coefficients used to calculate CS cross sections in this paper were determined using a one-channel optical model. However, one could argue that a coupled-channel model would be more appropriate for these nuclei (^{148,150,152}Sm) and that the scattering amplitudes from the CC model should be used to determine transmission coefficients for the WHF calculations. We shall demonstrate the scattering amplitudes that are found to represent the 13 measured elastic scattering differential cross sections and the total cross section are practically unique, independent of the optical model used. The definitions and relations used in this demonstration are those of Blatt and Weisskopf.[43]

The average transmission coefficient associated with the scattering amplitude of partial wave (j,l) is defined as

$$T_l^j \equiv 1 - |\overline{\eta}_l^j|^2 . \tag{A3}$$

$\overline{\eta}_l^j$ is the scattering amplitude averaged over fluctuations in energy; it is generally complex. T_l^j represents the fraction of incoming flux in channel l absorbed by the nucleus. Following Ref. 43 and ignoring the neutron's spin for illustrative purposes, the elastic scattering differential cross section and total cross section are given by

$$\sigma_{el}(\theta) = \pi\lambda^2 \sum_l (2l+1) P_l^2(\cos\theta) \overline{|1-\eta_l|^2} \tag{A4}$$

and

$$\sigma_t = 2\pi\lambda^2 \sum_l (2l+1)(1 - \mathrm{Re}\bar{\eta}_l) . \quad \text{(A5)}$$

Here again appropriate energy averages are indicated by the solidi.

$\sigma_{el}(\theta)$ can, when spin is included, be identified with the differential elastic cross sections measured in this experiment and σ_t with the known total cross section. Although these measured values do not uniquely determine the amplitudes η_l^j, they do severely constrain them. It has been suggested,[9] and we suggest here, that any optical model which represents the elastic scattering and total cross section will generate approximately the same $\bar{\eta}_l^j$, and hence T_l^j.

This supposition was tested for the case of 2.5 MeV neutrons on ^{152}Sm. At this energy we found T_l^j for the partial waves with $l > 4$ to be negligible. Transmission coefficients from the one-channel fit, shown in Fig. 5, and the coupled-channel fit, Fig. 8, are given in Table VII. They can be seen to be essentially the same. Disagreement in the coefficients for the p waves is associated with small differences in the calculated angular distributions for elastic scattering. We take the good agreement in Table VII as justification for using one-channel optical model transmission coefficients in our WHF calculations which are combined with CC cross sections in an effort to represent the measurements.

TABLE VII. Comparison of transmission coefficients determined using the one-channel model, Fig. 5, and the coupled-channel model, Fig. 8. Optical model parameters for these calculations are given in Table III.

j,l	$T(j,l)$ one-channel	$T(j,l)$ coupled-channel
$\frac{1}{2},0$	0.93	0.93
$\frac{1}{2},1$	0.51	0.56
$\frac{3}{2},1$	0.47	0.57
$\frac{3}{2},2$	0.90	0.92
$\frac{5}{2},2$	0.99	0.98
$\frac{5}{2},3$	0.20	0.24
$\frac{7}{2},3$	0.20	0.25
$\frac{7}{2},4$	0.12	0.12
$\frac{9}{2},4$	0.20	0.23
$\frac{9}{2},5$	0.00	0.00
$\frac{11}{2},5$	0.01	...

*Work supported in part by the National Science Foundation.

†Present address: Department of Radiology, George Washington University, Washington, D. C. 20007.

[1]D. F. Coope, M. C. Schell, S. N. Tripathi, and M. T. McEllistrem, Phys. Rev. Lett. 37, 1126 (1976).

[2]S. N. Tripathi, M. C. Schell, D. F. Coope, and M. T. McEllistrem (unpublished); for preliminary report see S. N. Tripathi, M. C. Schell, D. F. Coope, and M. T. McEllistrem, Bull. Am. Phys. Soc. 20, 1189 (1975); 21, 1004 (1976); M. C. Schell, M.S. thesis, University of Kentucky, 1976 (unpublished).

[3]A. W. Obst and J. L. Weil, Phys. Rev. C 7, 1076 (1973).

[4]P. Guenther and A. Smith, in *Nuclear Cross Sections and Technology*, edited by R. A. Schrack and C. D. Bowman, National Bureau of Standards Special Publications No. 425 (U.S. GPO, Washington, D.C., 1975), p. 862; L. Cranberg, in *Progress in Fast Neutron Physics*, edited by G. C. Phillips, J. B. Marion, and J. B. Risser (Univ. of Chicago Press, Chicago, 1963), p. 89.

[5]D. W. Glasgow and D. Graham Foster, Jr., Phys. Rev. C 3, 604 (1971); D. Graham Foster, Jr. and Dale W. Glasgow, *ibid.*, 3, 576 (1971).

[6]D. M. Chase, L. Wilets, and A. R. Edmonds, Phys. Rev. 110, 1080 (1958).

[7]R. E. Shamu, E. M. Bernstein, D. Blondin, J. J. Ramirez, and G. Rochau, Phys. Lett. 45B, 241 (1973).

[8]Ch. Lagrange, J. Phys. Lett. 35, 111 (1974).

[9]T. Tamura, Rev. Mod. Phys. 37, 679 (1965).

[10]R. E. Shamu, Ch. Lagrange, E. M. Bernstein, J. J. Ramirez, T. Tamura, and C. Y. Wong, Phys. Lett. 61B, 29 (1976).

[11]Ch. Lagrange, R. E. Shamu, T. Burrows, G. P. Glasgow, G. Hardie, and F. D. McDaniels, Phys. Lett. 58B, 293 (1975).

[12]M. T. McEllistrem, R. E. Shamu, J. Lachkar, G. Haouat, Ch. Lagrange, Y. Patin, J. Sigaud, and F. Coçu, Phys. Rev. C 15, 927 (1977).

[13]L. Cranberg, T. A. Oliphant, J. Levin, and C. D. Zafiratos, Phys. Rev. 159, 969 (1967); P. Marmier and E. Sheldon, *Physics of Nuclei and Particles* (Academic, New York, 1971), Vol. II, p. 1209.

[14]E. Sheldon and D. M. Van Patter, Rev. Mod. Phys. 38, 143 (1966).

[15]M. T. McEllistrem, J. D. Brandenberger, K. Sinram, G. P. Glasgow, and K. C. Chung, Phys. Rev. C 9, 670 (1974).

[16]A. T. G. Ferguson, I. J. van Heerden, P. Moldauer, and A. Smith, in *Proceedings of the International Conference on the Interactions of Neutrons with Nuclei*, Univ. of Lowell, Lowell, Mass. July, 1976, edited by Eric Sheldon (ERDA, Oak Ridge, 1976), CONF-760715-P1, p. 204.

[17]H. Feshbach and E. Sheldon, Phys. Today 30 (No. 2), 40 (1977).

[18]J. Barrette, M. Barrette, A. Boutard, R. Haroutunian, and G. Lamoureux, Phys. Rev. C 6, 1339 (1972).

[19]See discussion, Ref. 22, p. 202.

[20]See, e.g., F. D. McDaniels, J. D. Brandenberger,

G. P. Glasgow, and H. G. Leighton, Phys. Rev. C 10, 1087 (1974), and references cited therein.
[21]G. P. Glasgow, Ph.D. dissertation, University of Kentucky, 1974 (unpublished); G. P. Glasgow, F. D. McDaniels, J. L. Weil, J. D. Brandenberger, and M. T. McEllistrem (unpublished).
[22]M. T. McEllistrem, in *Proceedings of the International Conference on the Interaction of Neutrons with Nuclei* (see Ref. 16), p. 171.
[23]E. C. Hagen developed the peak fitting program.
[24]We used the value $\sigma_T = 1.05$ b at 2.47 MeV, taken from *MeV Total Neutron Cross Sections*, edited by R. D. Schwartz, R. A. Schrack, and H. T. Heaton, National Bureau of Standards Monograph No. 138 (U.S. GPO, Washington, D.C., 1964); also J. L. Fowler, C. H. Johnson, and R. M. Feezel, Phys. Rev. C 8, 545 (1973).
[25]C. A. Engelbrecht, Nucl. Instrum. Methods 80, 187 (1970).
[26]W. E. Kinney, Nucl. Instrum. Methods 83, 15 (1970).
[27]D. E. Velkley, D. W. Glasgow, J. D. Brandenberger, and M. T. McEllistrem, Nucl. Instrum. Methods 129, 231 (1975).
[28]E. H. Auerbach, BNL Report No. BNL 6562, Brookhaven National Laboratory, Upton, New York, 1962 (unpublished).
[29]J. Lachkar, M. T. McEllistrem, G. Haouat, Y. Patin, J. Sigaud, and F. Coçu, Phys. Rev. C 14, 933 (1976).
[30]L. Wolfenstein, Phys. Rev. 82, 690 (1951); W. Hauser and H. Feshbach, *ibid.* 87, 366 (1952).
[31]G. R. Satchler, Phys. Lett. 7, 55 (1963).
[32]P. A. Moldauer, Phys. Rev. C 12, 744 (1975).
[33]N. K. Glendenning, D. L. Hendrie, and O. N. Jarvis, Phys. Lett. 26B, 131 (1968).
[34]L. L. Riedinger, N. R. Johnson, and J. H. Hamilton, Phys. Rev. C 2, 2358 (1970).
[35]D. F. Coope, M. T. McEllistrem, M. C. Schell, and S. N. Tripathi, Bull. Am. Phys. Soc. 20, 1196 (1975); in *Proceedings of the International Conference on the Interaction of Neutrons with Nuclei* (see Ref. 16), p. 1326.
[36]G. Haouat, J. Sigaud, J. Lachkar, Ch. Lagrange, B. Duchemin, and Y. Patin, in *Proceedings of the International Conference on the Interaction of Neutrons with Nuclei* (see Ref. 16), p. 1330.
[37]D. L. Hendrie, Phys. Rev. Lett. 31, 478 (1973).
[38]See e.g. H. M. Hofmann, J. Richert, J. W. Tepel, and H. A. Weidenmüller, Ann. Phys. (N.Y.) 90, 403 (1975), and references therein.
[39]E. A. Andreev, V. K. Basenko, and S. P. Sit'ko, in *Proceedings of the International Conference on the Interaction of Neutrons with Nuclei* (see Ref. 16), p. 1334.
[40]J. W. Boring, Ph.D. dissertation, University of Kentucky, 1960 (unpublished).
[41]R. Chapman, W. McLatchie, and J. E. Kitching, Nucl. Phys. A186, 603 (1972).
[42]A. Gilbert and A. G. W. Cameron, Can. J. Phys. 43, 1446 (1965).
[43]J. M. Blatt and V. F. Weisskopf, *Theoretical Nuclear Physics* (Wiley, New York, 1957), p. 320.